Available online at www.sciencedirect.com
ScienceDirect
JOURNAL OF IRON AND STEEL RESEARCH, INTERNATIONAL. 2016, 23(3): 203-209

Recognition of Blast Furnace Gas Flow Center Distribution Based on Infrared Image Processing

Lin SHI[1], You-bin WEN[2], Guang-sheng ZHAO[2], Tao YU[1]
(1. School of Mathematics and Physics and Biological Engineering, University of Science and Technology of Inner Mongolia, Baotou 014010, Inner Mongolia, China; 2. School of Materials and Metallurgy, University of Science and Technology of Inner Mongolia, Baotou 014010, Inner Mongolia, China)

Abstract: To address the problems about the difficulty in accurate recognition of distribution features of gas flow center at blast furnace throat and determine the relationship between gas flow center distribution and gas utilization rate, a method for recognizing distribution features of blast furnace gas flow center was proposed based on infrared image processing, and distribution features of blast furnace gas flow center and corresponding gas utilization rates were categorized by using fuzzy C-means clustering and statistical methods. A concept of gas flow center offset was introduced. The results showed that, when the percentage of gas flow center without offset exceeded 85%, the average blast furnace gas utilization rate was as high as 41%; when the percentage of gas flow center without offset exceeded 50%, the gas utilization rate was primarily the center gas utilization rate, and exhibited a positive correlation with no center offset degree; when the percentage of gas flow center without offset was below 50% but the sum of the percentage of gas flow center without offset and that of gas flow center with small offset exceeded 86%, the gas utilization rate depended on both the center and the edges, and was primarily the edge gas utilization rate. The method proposed was able to accurately and effectively recognize gas flow center distribution state and the relationship between it and gas utilization rate, providing evidence in favor of on-line blast furnace control.

Key words: infrared image processing; gas flow center recognition; gas utilization rate; fuzzy C-means clustering

Blast furnace production is a series of complex physical, chemical and heat transfer reactions running under high temperature and high pressure conditions[1]. Since internal smelting is a typical dark-box operation[2-4], it is very difficult to achieve accurate real-time positioning and control of gas flow center distribution at blast furnace throat. Besides, a reasonable gas flow center distribution is an important condition that ensures steady descending of burden material and normal running of chemical reactions and heat exchange in the blast furnace[5-7], and an important route for smooth and stable running, energy conservation and consumption reduction, production increase and quality improvement of the blast furnace. Therefore, to have accurate real-time information of gas flow center distribution and to determine the relationship between gas flow center distribution features and gas utilization rate are vital to blast furnace production control.

Conventional blast furnace operation is adjusted and controlled by the furnace superintendent through empirical judgment of the blast furnace gas flow distribution. In recent years, many scholars have studied gas flow recognition methods, primarily including (1) building a mechanism model for gas flow distribution by the rules of gas moving in burden layers[8,9], which is very complicated in computation and too difficult to obtain the rules of burden layer motion; (2) building a neural network model based on cross temperature measurement data in order to recognize blast furnace gas flow distribution mode[10,11], which primarily recognizes burden surface temperature and is not able to reflect the distribution location of gas flow center accurately and in real-time; (3) the laser[12] and ultrasonic[13] methods which are used to test the shape and temperature of the burden

Foundation Item: Item Sponsored by National Natural Science Foundation of China (61263015)
Biography: Lin SHI, Doctor, Professor; **E-mail**: shilin_dingyan@sina.com; **Received Date**: January 9, 2015

surface, but regardless of the gas flow distribution; (4) using infrared camera to observe development of gas flow over burden surface in modern blast furnaces along with developing infrared technology[14,15]. Wu et al.[16] conducted data fusion with infrared images and cross temperature measurements, mainly studied gas flow development and distribution in terms of gas flow index, but had no in-depth study on specific distribution features of gas flow center and the influences of such center distribution on blast furnace production.

In this paper, a 2500 m^3 blast furnace was the subject of present study (with raw material from Bayan Obo Mine). Infrared video data of production was acquired on-line for 1 month (720 h), and through batch processing of massive infrared image data, 3600 frames of infrared images of gas flow per hour were obtained. The distribution features of gas flow center every hour were recognized (i.e., 720 h, 3600 frames of image per hour) and statistically quantified, and with taking cross temperature measurement data into account, the fuzzy C-means clustering method was employed to categorize blast furnace gas flow center distribution and gas utilization rate, and to determine their relationship.

1 Image Processing

It can be known from infrared imaging principle that the intensity of infrared light is proportional to temperature. It can be known from the radial distribution of gas flow temperature at blast furnace throat that, the stronger the gas flow, the higher the temperature and the larger the bright zone of film; the weaker the gas flow, the lower the temperature, and consequentially the bright zone of image is very small or even absent. Thereby the infrared images were recognized according to this principle.

1.1 Image filtering

Since blast furnace iron smelting is a highly complex process, infrared images easily produce noises and pulse interference which are detrimental to extraction of image features, so they have to be filtered. Image filtering methods include Gaussian filtering, median filtering and mean filtering; as Gaussian filtering is mainly used to filter Gaussian noise while individual median or mean filtering has no significant effect, the images were mainly processed with a combination of mean filtering[17] and median filtering[18] in this paper. The specific procedure is as follows:

Step 1 Select one infrared image and thus acquire $g(x,y)$, where x is the row number of an image, and y is column number of the image.

Step 2 Process the infrared image $g(x,y)$ using mean filtering and save it to the image $g_1(x,y)$, i.e.

$$g_1(x,y)=\frac{1}{9}\sum_{(x,y)\in(3\times3)}g(x,y) \tag{1}$$

Step 3 For the mean-filtered image, $g_1(x,y)$ run median filtering and save it to the image $f(x,y)$, where the value of $f(x,y)$ is the grayscale of the pixel (x,y).

Figs. 1(a) and 1(b) are the original image and the filtered image respectively. After mean and median filtering of an image, not only some glitches and salt-and-pepper noise are removed, but also the image is smoothed, thus overcoming stochastic interference effectively and retaining image details and edges relatively well; moreover, the burden surface temperature information is preserved in the form of grayscale image, providing the basis for image feature extraction.

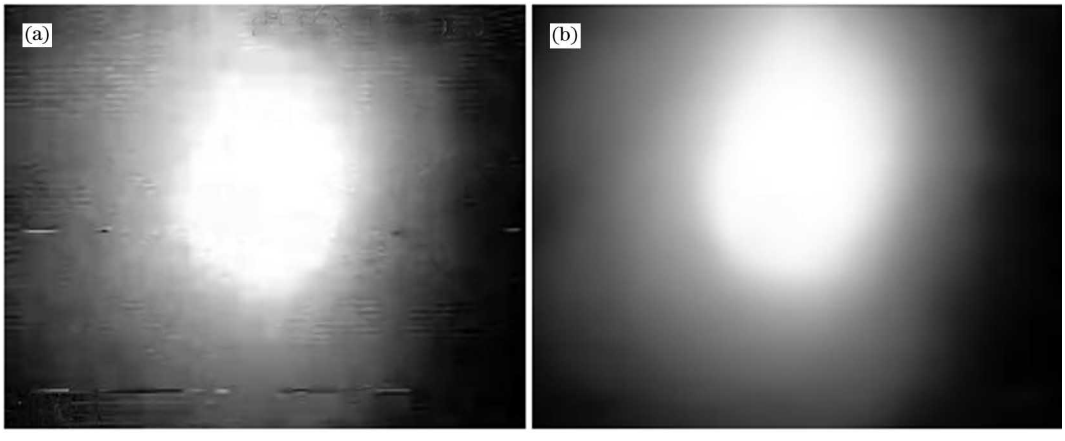

(a) Original grayscale image; (b) Mean and median filtered image.

Fig. 1 Image filtering

1.2 Image feature extraction

In this paper, total threshold segmentation method was used to segment threshold of the filtered images. Set a threshold T for image segmentation, the derived image after segmentation is $F(x,y)$:

$$F(x,y)=\begin{cases}1, & f(x,y)>T\\ 0, & f(x,y)\leqslant T\end{cases} \tag{2}$$

Hence, a grayscale image is converted into a binary image through threshold segmentation[19], as shown in Fig. 2.

Fig. 2 The image after threshold segmentation

2 Calibration of Temperature Field

To obtain a correlation between temperature and grayscale, it is necessary to determine corresponding positions of cross temperature-measuring thermocouples in the infrared image[20], their grayscales and temperatures.

2.1 Spatial calibration

To determine positions of the blast furnace physical center and cross temperature-measuring thermocouples in an infrared image, it is necessary to perform spatial calibration. An infrared camera is securely mounted in a hole drilled in furnace wall at the furnace top so as to take images of furnace interior. When the camera is shooting an image of burden surface inside the blast furnace, a certain shooting distance and inclined angle exist between the camera lens and the burden surface; as a result, the obtained infrared image has certain tilting distortion. To determine positions of cross temperature-measuring thermocouples in an image, the shot burden surface inside blast furnace has to be rotated, as shown in Fig. 3, where O_1 is the position of the infrared camera, and O_2 is the rotation center; through rotation, the radial length MN of burden surface QH in the image can be obtained.

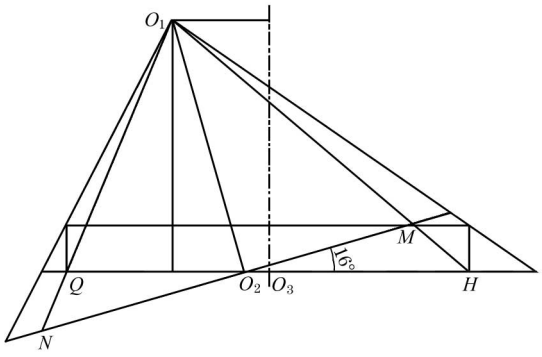

Fig. 3 Infrared shooting plane

The deeper the furnace burden level, the more mixed the rising gas and the lower the accuracy of cross temperature measurement; thus, calibration of cross temperature measurements in case of high burden level is a necessary condition for improving infrared inspection accuracy. In this paper, the data of burden level at 1 m of the blast furnace were calibrated, and the calculation yielded a correlation between burden surface and infrared image. Specifically, every pixel on vertical axis of the infrared image represents a length of 36 mm, and the number of pixels between every two cross temperature-measuring thermocouples is 19; every pixel on horizontal axis represents a length of 24 mm, and the number of pixels between every two cross temperature-measuring thermocouples is 29; the vertical distance between blast furnace physical center and image center is 14 pixels while the horizontal distance is 0. Thereby, the positions of the furnace cross temperature-measuring thermocouples in an infrared image can be determined, as shown in Fig. 4. No. 6 is the position of furnace physical center in the image, Nos. 1-11 are horizontal positions of the southeast-to-northwest thermocouples in the image, and Nos. 12-21 are ver-

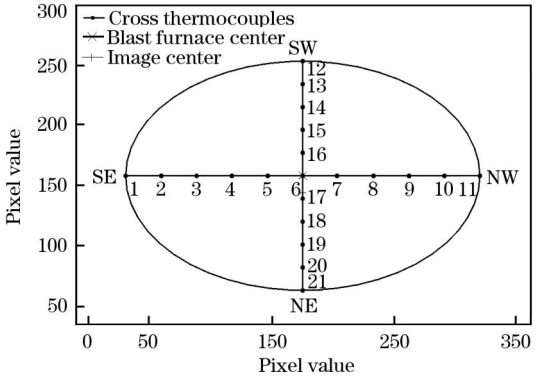

Fig. 4 Positions of cross temperature-measuring thermocouples

tical positions of the southwest-to-northeast thermocouples in the image.

2.2 Calibration of temperature and grayscale

Based on the reference temperature values measured by cross temperature-measuring thermocouples and depending on positions of cross temperature-measuring thermocouples in each infrared image, a statistical analysis yields the grayscale values near cross temperature-measuring thermocouples in the image (Table 1). As Nos. 1 and 11 are the thermocouples near the edges, the temperatures they measured are higher than those measured by thermocouples 2 and 10, and a scatter plot indicates that there is an approximately linear relationship between reference temperature and corresponding reference grayscale within local range, as shown in Fig. 5.

A correlation between temperature and grayscale was obtained by means of least-squares linear regression, and the regression model passed statistical test of regression parameters and regression equation (Table 2). Eq. (3) is the regression equation. This regression equation provides the basis for subsequent gas flow center distribution recognition in this paper.

$$y = 0.5842x - 84.5784 \quad (3)$$

Table 1 Reference temperatures and corresponding reference grayscale values

	1	2	3	4	5	6	7	8	9	10	11
Reference temperature value (x)	257	139	358	452	508	584	486	426	321	106	223
Reference grayscale value (y)	36	0	146	182	224	247	196	161	125	0	8

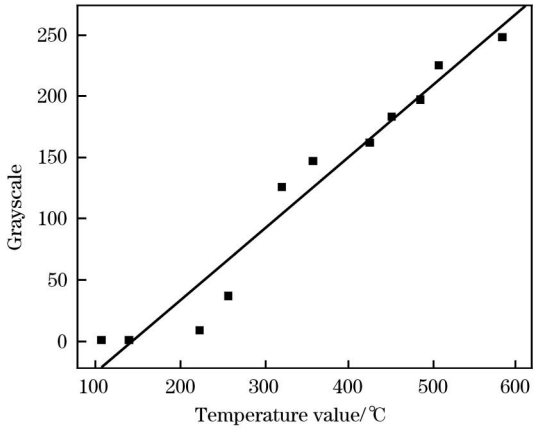

Fig. 5 Fitting plot of temperature versus grayscale

Table 2 Significance test of regression model coefficients

Coefficient	Estimate	Standard error	t value	Pr ($>\|t\|$)
Intercept	−84.5784	16.3166	−5.152	0.000578
X	0.5842	0.0428	13.649	2.55×10^{-7}

3 Gas Flow Center Distribution Recognition

It can be known from actual blast furnace production conditions that variable gas flow center distribution is able to reflect operating state of a blast furnace and its gas utilization rate. The temperature calibration indicates that the grayscale of infrared image is able to reflect gas flow distribution state. Therefore, extracting features of gas flow centers in infrared images and recognizing gas flow center distribution mode are able to reflect effectively actual distribution state of gas flow center on burden surface, which is more beneficial for guidance of furnace burden distribution operation.

3.1 Gas flow center feature extraction

The high-temperature zone in gas flow on burden surface at blast furnace throat is a zone of vigorous gas flow, i.e., the area where gas flow center is situated. The correlation between temperature and grayscale shows that gas flow temperature exceeds 500 ℃ when grayscale is greater than 220; in other words, this is a high-temperature zone. Therefore, the threshold scope of gas flow center in an image was set as a zone with grayscale values above 220. After threshold segmentation of an image, a binary image was obtained, with a bright zone having grayscale value above 220. Depending on bitmap stream format of an image, it is supposed that the coordinates of the left bottom corner and the right top corner are (0, 0) and (351, 287) respectively, and averaging all abscissae and ordinates in the bright zone respectively yields the coordinates of the center of bright zone, i.e., the gas flow center in the image. And in individual images, all grayscale values are smaller than 220, indicating that the gas flow center is not apparent at this time; thus, no extraction was done.

3.2 Gas flow center distribution recognition

To depict distribution of gas flow center per hour, the positions of the furnace physical center and cross temperature-measuring thermocouples were deter-

mined in the grayscale images though spatial calibration. With the vertical pixels between two vertical neighboring cross temperature-measuring thermocouples in the image as the minor semiaxis, the horizontal pixels between two horizontal neighboring cross temperature-measuring thermocouples as the major semiaxis, and the position of furnace physical center in the image as the center, five ellipses could be plotted in the image to represent approximately the actual burden surface temperature field. Marking the extracted coordinates of gas flow image centers on the ellipses yields the variation in position of gas flow center per hour inside the blast furnace.

In this paper, 720-hour infrared video data were acquired from a blast furnace and batch processed to be finally converted to infrared image data (1 frame per second). Every frame of image was mean and median filtered, followed by extraction of gas flow center features to obtain the distribution state of gas flow center on the ellipses per hour (totally 720 h). Fig. 6 shows four distribution features of gas flow center at a certain time of 720 h. A concept of "gas flow center offset" was introduced to facilitate description. There were three rings of ellipses from inner side to outer side; the points falling within the first ring were called "gas flow center without offset", the points falling within the second ring were called "gas flow center with small offset", and the points falling within the third ring were called "gas flow center with large offset". By using Eq. (4), the percentage of points falling within any of these three ellipses per hour was calculated, while the statistical results of the data in Fig. 6 is shown in Table 3.

$$r_{ie}=\frac{N_{ie}}{N_e},\ i=1,2,3;\ e=1,2,\cdots,720 \tag{4}$$

where, N_e is the total number of gas flow center points extracted at the eth hour; N_{ie} is the number of center points falling within the ith ring at the eth hour; and r_{ie} is the percentage of gas flow center falling within the ith ring at the eth hour. With reference to Table 3, Fig. 6(a) shows that the gas flow centers are mainly distributed within the first ring and the percentage reaches 85.6%, indicating that the furnace gas flow center shifts very little and the vigorous gas flow zone focuses on the center of furnace throat; Fig. 6(b) shows that the gas flow centers are mainly distributed within the second ring and the percentage reaches 71.78%, indicating that the furnace gas flow center shifts relatively slightly and a majority of the vigorous gas flow zone deviates

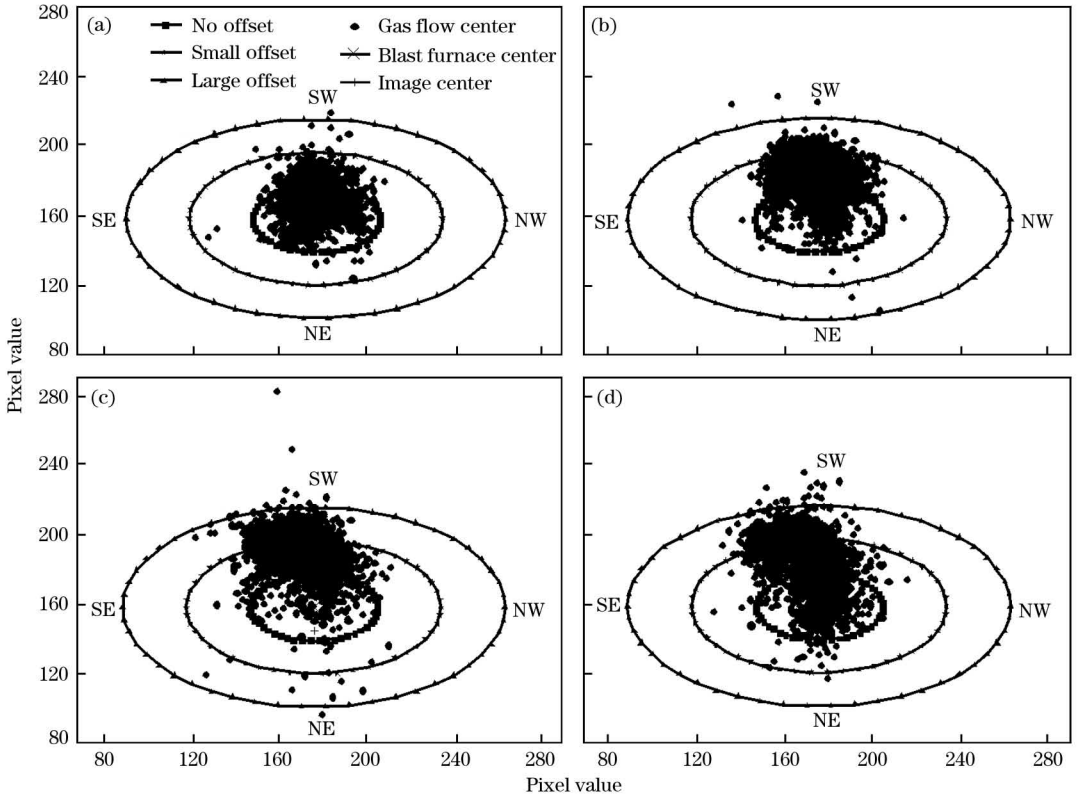

(a) The centers are concentrated in no-offset zone; (b) The centers are concentrated in a small-offset zone; (c) The centers are concentrated in a large-offset zone; (d) The centers are evenly distributed.

Fig. 6 Distribution of gas flow center points

Table 3 Statistical results of center points in a 4-hour period

	Number of center points				Inconspicuous center	Percentage of center points			
	N_{1e}	N_{2e}	N_{3e}	Beyond the third ring		r_{1e}	r_{2e}	r_{3e}	Beyond the third ring
Fig. 6(a)	2744	446	13	2	395	0.8560	0.1390	0.0042	0.0007
Fig. 6(b)	580	2139	258	3	620	0.1946	0.7178	0.0866	0.0010
Fig. 6(c)	269	1280	1443	13	595	0.0895	0.4260	0.4802	0.0043
Fig. 6(d)	672	1209	898	16	850	0.2404	0.4326	0.3212	0.0057

from the center of furnace throat; Fig. 6(c) shows that more gas flow centers are distributed within the third ring and the percentage reaches 48.02%, indicating that the furnace gas flow center shifts much and the vigorous gas flow zone deviates greatly from the center of furnace throat. Fig. 6(d) shows that gas flow centers are relatively uniform and their percentages within the first, second and third rings are about 30%, indicating that gas flow center shifts but the offset is relatively uniform. As seen from Fig. 6, the furnace gas flow center mainly shifts southwestward. This phenomenon is matching with the actual production of blast furnace, as shown in Fig. 7. In this paper, a vector was used to characterize distribution state of furnace gas flow center during the eth hour.

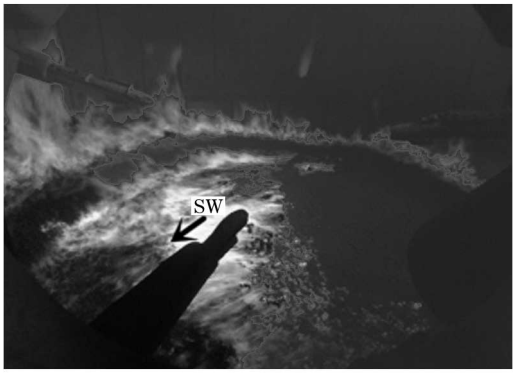

Fig. 7 The photo of gas flow distribution in actual production of blast furnace

4 Fuzzy C-means Clustering Analysis

In practical blast furnace production, gas utilization rate is an important indicator of blast furnace operating state, and one main influential factor of gas utilization rate is burden surface distribution; in turn, various gas flow center distributions are real-time representation of the states of different burden surfaces in furnace throat. Therefore, different gas flow center distributions correspond to different gas utilization rates, and exploring and analyzing their statistical rules is of significant importance to guidance on blast furnace burden distribution operation. In this paper, fuzzy C-means clustering method[21] was used for classification study.

4.1 Principles of fuzzy C-means clustering

In this paper, gas flow center offset $\vec{r}_e=\{r_{1e}, r_{2e}, r_{3e}\}$ per hour and corresponding gas utilization rate C_e were grouped into 720 vectors $\{\vec{\beta}_e \mid \vec{\beta}_e=\{r_{1e}, r_{2e}, r_{3e}, C_e\},\ e=1,2,\cdots,720\}$ which serve as the samples for fuzzy clustering. The clustering loss function J_f defined in terms of membership function is:

$$J_f=\sum_{j=1}^{c}\sum_{i=1}^{720}[u_i(\vec{\beta}_i)]^b \parallel \vec{\beta}_i-\vec{m}_j \parallel^2 \tag{5}$$

where, c is the number of types predetermined; $\vec{m}_j$ $(j=1,2,\cdots,c)$ is the clustering center; b is a constant which can control the fuzzy degree of clustering results, and $b=2$ in practice based on experimental data; and $u_j(\vec{\beta}_i)$ is the membership function of sample i for type j, $u_j(\vec{\beta}_i)\in(0,1)$, and $\sum_{j=1}^{c}u_j(\vec{\beta}_i)=1$, $i=1,2,\cdots,720$. Following equations can be obtained by finding extrema of Eq. (5):

$$\vec{m}_j=\frac{\sum_{i=1}^{720}[u_j(\vec{\beta}_i)]^2\vec{\beta}_i}{\sum_{i=1}^{720}[u_j(\vec{\beta}_i)]^2} \tag{6}$$

$$u_j(\vec{\beta}_i)=\frac{[1/\parallel \vec{\beta}_i-\vec{m}_j \parallel^2]^{1/(b-1)}}{\sum_{k=1}^{c}[1/\parallel \vec{\beta}_i-\vec{m}_k \parallel^2]^{1/(b-1)}}$$
$$i=1,2,\cdots,720;\ j=1,2,\cdots c \tag{7}$$

4.2 Results and analysis

The clustering results of this study are shown in Table 4.

These four types of results in Table 4 allow one

Table 4 Results of fuzzy C-means clustering %

Type	Gas flow center without offset	Gas flow center with small offset	Gas flow center with large offset	Average gas utilization rate
1	85.38	13.32	0.44	41.86
2	67.01	31.46	1.43	39.00
3	50.06	45.87	3.92	37.96
4	28.18	58.43	13.18	38.32

to determine the relationship between gas flow center distribution and gas utilization rate fairly well. (1) Comparison between type 1 and type 2, type 3 or type 4 shows that, the average furnace gas utilization rate is above 41% when the percentage of gas flow center without offset exceeds 85%, indicating that the gas utilization rate is the maximum when gas flow center is distributed at the center of furnace throat. (2) Table 4 shows that gas utilization rate is positively correlated with no center offset degree when more than 50% of gas flow center points have no offset. In other words, the smaller the center offset, the higher the average gas utilization rate, indicating that the center gas utilization rate is predominant at this time. (3) Comparison between type 3 and type 4 shows that, the percentage of type 4 gas flow center without offset (28.18%) is obviously lower than that of type 3 (50.06%) while gas utilization rate of type 4 (38.32%) is greater than that of type 3 (37.96%), indicating that gas utilization rate is determined by center and edge development altogether during blast furnace operation, and edge gas utilization rate is predominant.

5 Conclusions

(1) Combining furnace infrared images and cross temperature measurements, use of the least squares regression method enables more accurate determination of temperature versus grayscale correlation, achieving grayscale-to-temperature conversion.

(2) When burden surface temperature field information is reflected by infrared images, batch processing of massive data from image filtering and gas flow center feature recognition succeeds in extracting the variation information of gas flow center per second.

(3) As a concept of "gas flow center offset" is introduced, classification of vectors composed of gas flow center offset per hour and corresponding gas utilization rate using fuzzy C-means clustering method indicates that the average furnace gas utilization rate reaches 41% when the percentage of gas flow center without offset exceeds 85%; the gas utilization rate is positively correlated with no center offset degree when the percentage of gas flow center without offset exceeds 50%, and center gas utilization rate is predominant; and when the percentage of gas flow center without offset is small but the sum of the percentage of gas flow center without offset and that with small offset exceeds 86%, gas utilization rate is jointly determined by center and edge development, and predominantly by edge gas flow center.

(4) In blast furnace production, on-line monitoring of gas flow center offset degree and position coupled with gas utilization rate to guide on burden distribution operation is able to improve development of gas flow center and edges at furnace throat, so as to improve gas utilization rate and eventually achieve visual operation and on-line control of furnace burden distribution.

References:

[1] C. Saxena, S. Prasad, A. Lavanya, S. Thakur, K. Suresh Kumar, Ironmak. Steelmak. 34 (2007) 5-9.

[2] L. Y. Wen, C. G. Bai, Y. Q. Ou, D. F. Chen, J. Iron Steel Res. Int. 13 (2006) No. 2, 18-21.

[3] M. S. Chu, X. F. Yang, F. M. Shen, J. I. Yagi, H. Nogami, J. Iron Steel Res. Int. 13 (2006) No. 6, 8-15.

[4] X. F. Dong, A. B. Yu, J. I. Yagi, P. Zulli, ISIJ Int. 47 (2007) 1553-1570.

[5] X. F. Dong, D. Pinson, S. J. Zhang, A. B. Yu, P. Zulli, Appl. Math. Modell. 11 (2006) 1293-1309.

[6] M. Nikus, H. Saxén, ISIJ Int. 36 (1996) 1142-1150.

[7] R. Timmer, J. Droog, G. Flierman, A. Steeghs, Steel Res. 68 (1997) 47-53.

[8] K. Takatani, T. Inada, Y. Ujisawa, ISIJ Int. 39 (1999) 15-22.

[9] J. Jimenez, J. Mochón, A. J. S. De, ISIJ Int. 44 (2004) 518-526.

[10] Y. Otsuka, M. Konishi, K. Hanaoka, T. Maki, ISIJ Int. 39 (1999) 1047-1052.

[11] J. Hinnelä, H. Saxén, F. Pettersson, Ind. Eng. Chem. Res. 42 (2003) 2314-2323.

[12] Y. F. Zhao, J. C. Capo, S. J. McKnight, J D′Alessio, K. J. Ferron, P. F. Badgley, Z. K. Gao, T. Gao, Iron Steel Technol. 8 (2011) No. 1, 52-61.

[13] Q. Zhu, C. L. Lü, Y. X. Yin, X. Z. Chen, J. Iron Steel Res. Int. 20 (2013) No. 6, 33-37.

[14] A. Bulsari, H. Saxen, Steel Res. Int. 66 (1995) 231-236.

[15] J. Jimenez, J. Mochón, A. Formoso, ISIJ Int. 40 (2000) 114-120.

[16] M. Wu, C. J. Wang, J. Q. An, Y. He, Information and Control 40 (2011) No. 1, 79-82.

[17] M. Grundland, N. A. Dodgson, Pattern Recogn. 40 (2007) 2891-2896.

[18] P. E. Ng, K. K. Ma, IEEE T. Image Process. 15 (2006) 1506-1516.

[19] J. Sauvola, M. Pietikäinen, Pattern Recogn. 33 (2000) 225-236.

[20] F. Pettersson, H. Saxén, K. Deb, Mater. Manuf. Process. 24 (2009) 343-349.

[21] T. Velmurugan, Appl. Soft Comput. 19 (2014) 134-146.